A Complete Electromagnetic Simulation of the Separated-Aperture Sensor for Detecting Buried Land Mines

Jacqueline M. Bourgeois, *Member, IEEE*, and Glenn S. Smith, *Fellow, IEEE*

***Abstract*—The detection of buried land mines is a problem of military and humanitarian importance. Electromagnetic sensors (ground-penetrating radars) use signals at radio and microwave frequencies for this purpose. In the past, electromagnetic sensors for land-mine detection have been empirically developed and optimized. This has involved experimental tests that are complicated, time consuming, and expensive. An alternative, which has only recently become available, is to carry out initial development and optimization using accurate numerical simulations. One objective of this paper is to show, for the first time, that such simulations can be done using the finite-difference time-domain (FDTD) method. The separated-aperture sensor has been under investigation by the United States Army for land-mine detection for many years. It consists of two parallel dipole antennas housed in corner reflectors that are separated by a metallic septum. It is a continuous-wave sensor tuned to a particular frequency (typically 790 MHz). When the sensor is over empty ground, the coupling between the antennas is very small. As the sensor is moved over a buried mine, the coupling between the antennas increases indicating the presence of the mine. In this paper, the complete electromagnetic system composed of the separated-aperture sensor, air and soil, and buried land mine is modeled using the FDTD method. The finite computational volume is truncated with an absorbing boundary condition: the generalized perfectly matched layer. Detailed studies made with the simulation increase the understanding of this sensor. Results computed from the simulation are in good agreement with experimental measurements made at Georgia Tech and with measurements made by the United States Army.**

***Index Terms*—Buried object detection, FDTD methods, ground-penetrating radar, land mine terms.**

I. Introduction

LAND mines are explosive devices placed on or beneath the surface of the earth for the purpose of destroying vehicles and killing or maiming human beings. Mines are usually deployed during a military conflict; however, they may remain in the ground undetected for decades after the cessation of hostilities. The United Nations estimates that there are currently over 100 million land mines buried in 62 countries throughout the world, and that the number of deployed mines increases by approximately 2 million each year [1]. Accidental detonation of mines kills or maims 600 or more people a month, predominantly civilians. The resulting injuries have devastating effects on the lives of the wounded and place incredible demands on the health, welfare, and social systems of the nations involved. There is presently no reliable means for detecting these hidden mines.

Since World War II, the United States Army has investigated many different technologies for detecting land mines [2]–[4]. These include the use of electromagnetic radiation over a wide spectrum: very low frequencies (metal detectors), radio and microwave frequencies, infrared and optical frequencies. The sensors operating at radio and microwave frequencies are often in the form of a ground-penetrating radar (GPR), and it is this type of sensor that is investigated in this paper.

The composition of land mines is variable, ranging from those that contain a significant amount of metal (a metal case filled with explosive) to those that are essentially all dielectric (a plastic case filled with explosive). Metal detectors can be used to find the former but not the latter. Thus, an important requirement for an electromagnetic sensor operating at a radio or microwave frequency (a GPR) is the ability to detect all-dielectric (nonmetallic) mines, even in situations where the electrical properties (specifically the relative permittivity) of the mine are close to those of the surrounding soil [5].

In the past, electromagnetic sensors for land-mine detection have been empirically developed and optimized. This has involved experimental tests that are complicated, time consuming, and expensive. An alternative is to carry out initial development and optimization using theoretical simulations. Because of the close proximity and strong electromagnetic coupling of the sensor, earth, and mine, such simulations must be for the complete system, not an isolated element, such as an antenna in free-space. Numerical methods, because of their flexibility, offer the best approach to this problem. However, until recently, such numerical simulations were not possible for a problem this complicated because of the limitations on computer memory and speed. One objective of this paper is to show for the first time that a complete three-dimensional (3-D) electromagnetic simulation for an actual mine-detection sensor can produce results comparable to those obtained from accurate experimental measurements.

Manuscript received May 27, 1997; revised March 27, 1998. This work was supported in part by the Joint Services Electronics Program under Contracts DAAH04-93-G-0027 and DAAH04-96-1-0161, by the Army Research Office under Contract DAAH04-94-G-0144, and by the University of Minnesota High-Performance Computing Research Center under Contract DAAL03-89-C-0038.

J. M. Bourgeois was formerly with the School of Electrical and Computer Engineering, Georgia Institute of Technology, Atlanta, GA. She is now with Raytheon Electronic Systems Co., Missile Radar Laboratory, Sudbury, MA 01776 USA.

G. S. Smith is with the School of Electrical and Computer Engineering, Georgia Institute of Technology, Atlanta, GA 30332 USA.

Publisher Item Identifier S 0018-926X(98)07488-2.

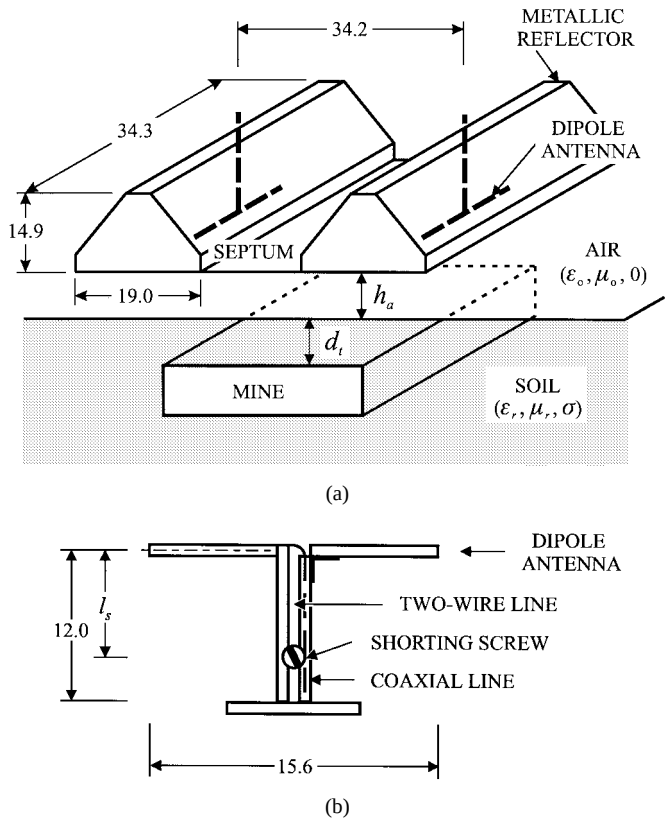

Fig. 1. (a) Separated-aperture sensor for detecting buried land mines. (b) Detail of dipole antenna. Sensor is designed for 790 MHz and all dimensions are in centimeters.

Fig. 1(a) shows the electromagnetic sensor considered in this paper. It has been under investigation by the United States Army for many years and has been given various names: "separated-aperture sensor," "waveguide beyond cutoff sensor," PRS-6, etc. [3], [4]. Most recently, this sensor was studied experimentally by L. S. Riggs and C. A. Amazeen at the United States Army Belvoir Research, Development and Engineering Center [6]. In this paper, the separated-aperture sensor is analyzed using the finite-difference time-domain (FDTD) numerical method for solving Maxwell's equations [7], [8]. The finite computational volume, which contains the sensor, ground, and mine, is truncated with an absorbing boundary condition (ABC): the generalized perfectly matched layer (GPML) of Fang and Wu [9]. This boundary condition effectively absorbs waves incident at all angles from the air (lossless medium) and from the earth (lossy medium). The computations are performed on a massively parallel supercomputer [the Connection Machine-5 (CM-5)] at the Army High-Performance Computing Research Center (AHPCRC) at the University of Minnesota.

Section II of this paper describes the separated-aperture sensor. Section III describes the FDTD simulation of the complete mine-detection problem (sensor, ground, and targets) and shows some results from FDTD studies of the sensor performance. Section IV describes validation of the FDTD simulation; FDTD results are shown to be in good agreement with results obtained using a separated-aperture sensor constructed and measured at Georgia Tech and with the aforementioned measurements made by the United States Army at Fort Belvoir.

II. Separated-Aperture Sensor

The separated-aperture sensor shown in Fig. 1(a) consists of two parallel dipole antennas housed in corner reflectors that are separated by a metallic septum. When the sensor is over empty ground, the coupling between the antennas ($|S_{21}|$) is very small. As the sensor is moved over a buried target, the target reflects a portion of the signal radiated by the transmitting antenna back to the receiving antenna, thus increasing the coupling between the antennas. The increase in coupling is used to detect the presence of the buried target.

Fig. 1 gives the dimensions for the components of a separated-aperture sensor (corner reflectors, septum, and dipole antennas with feeding/matching structures) designed to operate at 790 MHz.[1] As shown in Fig. 1(b), each dipole antenna is attached to a corner reflector with two parallel conductors that form a two-wire transmission line (characteristic impedance $Z_c \approx 116\Omega$). One of these conductors contains a coaxial line used to feed the dipole. At the top end, the inner and outer conductors of the coaxial line are attached to separate arms of the dipole and, at the bottom end, the coaxial line is attached to a source. The two-wire transmission line also acts as a tuning stub; the position of the shorting screw l_s is adjusted to change the length of the stub and match the impedance of the dipole to the characteristic impedance of the feeding coaxial line.

Some characteristics of the separated-aperture sensor are illustrated by results from the experimental study performed by the United States Army [6]. In that study, measurements were made with the sensor at various heights over empty ground, and at the same heights over ground containing a target buried at various depths. Fig. 2 shows results for the sensor 7.6 cm above the ground with the target buried at a depth of 7.6 cm. These data were obtained by digitizing the curves in [6].

The soil for the above experiments is described as a "fairly dry, loamy soil with moisture content by weight of 6%." The electrical properties of the soil, which were measured using a coaxial line method, are reported to be $\varepsilon_r = 2.9$, $\mu_r = 1.0$, $\sigma = 0.02$ S/m. The target is a nylon block ($30.5 \times 30.5 \times 7.6$ cm) with $\varepsilon_r = 3.16$, $\mu_r = 1.0$, $\sigma \approx 0$, chosen because it has properties similar to those of nonmetallic land mines.

Fig. 2(a) shows the standing-wave ratio (SWR) for the transmitting antenna when the sensor is over empty ground. Notice that the antenna is matched near 790 MHz; the SWR is a minimum (1.5) at 785 MHz. Fig. 2(b) shows the coupling between the antennas ($|S_{21}|$) for the sensor over empty ground (lines with solid circles) and for the sensor centered over the buried target (lines with hollow circles). Notice that $|S_{21}|$ peaks near 790 MHz in both cases, and that there is a detectable increase in the coupling (about 15 dB at 790 MHz) as the sensor is moved over the buried target. This case represents a rather severe test for the sensor; the

[1] These are the dimensions for the sensor discussed in Section IV-A, which was fabricated at Georgia Tech. They are similar to the dimensions of the United States Army sensor described in [6].

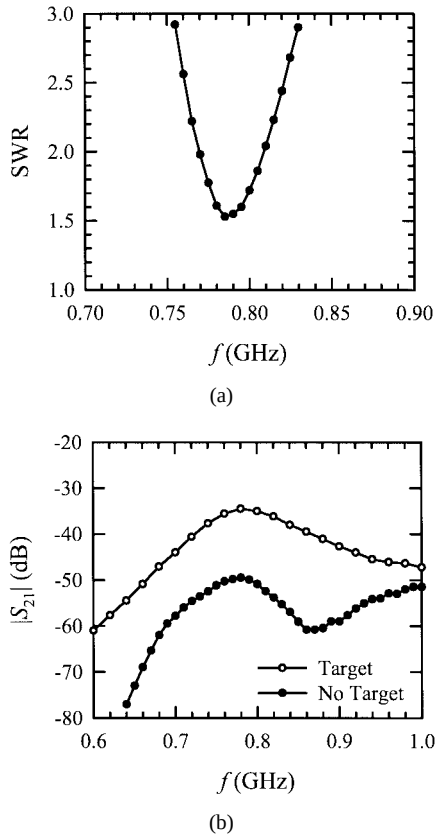

Fig. 2. United States Army measurements with a separated-aperture sensor at height $h_a = 7.6$ cm over soil. (a) SWR. (b) $|S_{21}|$ for sensor over empty soil (no target) and over soil containing a nylon block buried at depth $d_t = 7.6$ cm. Measured data from [6].

relative permittivity of the nylon target is close to that of the surrounding soil, $\varepsilon_r = 3.16$ versus $\varepsilon_r = 2.9$. The relative permittivity of the target is also higher than that of the surrounding soil; a condition that is specific to very dry soils.

Until now, there has been no comprehensive theoretical analysis of the separated-aperture sensor. However, the following qualitative explanation for its operation was offered some time ago [4]. The space between the metallic septum and the surface of the ground can be viewed as an air-filled waveguide. Because of the orientation of the dipoles, the electric field in this waveguide will be predominantly parallel to the septum and the surface of the ground. When the height of the sensor h_a is small, the field (modes) within the waveguide will be cut off.[2] Thus, there will be exponential decay of the field within the waveguide and very little coupling between the dipoles. When a target is in the soil below the sensor, electromagnetic energy scattered from the target increases the coupling between the dipoles. The target can be thought of as a perturbation to the structure for the waveguide.

III. FDTD Simulation

A. Computational Model

The FDTD simulation is a complete 3-D model of the mine-detection problem with full electromagnetic models of all aspects of the sensor, target, and soil. The numerical simulation uses a volume of size $1.024 \times 1.024 \times 1.024$ m, which is comprised of cubic Yee cells of dimension 0.4 cm [7]. Field components are updated every $\Delta t = 6.67$ ps; this time step satisfies the condition for numerical stability [8].

The metallic components (antennas, stubs, corner reflectors, and septum) are modeled as perfect electric conductors (PEC's). The slanted edges of the corner reflectors are approximated using staircasing. The lengths of the dipole antenna and stub are as shown in Fig. 1(b). The radii of the dipole arms and of the parallel wires of the stub are less than a half of a cell's width; therefore, they cannot be included using the usual FDTD update equations. The magnetic field update equations are modified along the axes of the dipole arms and parallel wires to account for field variations near a thin, circular wire, as described in [10]. The ratio of the radius to separation distance for wires of the stub is chosen to yield the desired characteristic impedance ($Z_c \approx 116\Omega$) of the two-wire line. On the stub, a shorting plate is used in place of the shorting screw shown in Fig. 1(b), because the geometry of the plate (a box) is easier to model than that of the screw (a cylinder), and its performance is equivalent.

The feeding of both the transmitting and receiving antennas is accomplished using a simple, one-dimensional (1-D) FDTD model of a transmission line such as that described in [11]. The 1-D feed is attached to the 3-D grid at the terminals of the dipole antenna. It replaces the coaxial line shown in Fig. 1(b). A differentiated Gaussian pulse is introduced into the transmission line of the transmitting antenna using a one-way source positioned 15 cells before the point of attachment to the 3-D grid. The differentiated Gaussian pulse is of the form

$$\mathcal{V}(t) = V_o(t/\tau_p)\, e^{-t^2/2\tau_p^2} \tag{1}$$

where $V_o = 1000$ V, $\tau_p = 0.25$ ns. The frequency spectrum of this signal is maximum near 790 MHz. The Fourier transform of the output of a single FDTD run with this pulse produces data over the range of frequencies of interest.

The boundaries of the FDTD volume are terminated using a GPML eight cells thick that is backed by a PEC [9]. The electric and magnetic conductivities within the layer are a parabolic function of the distance from the surface of the GPML; the conductivities increase smoothly from the surface of the GPML to the back PEC. Within the layer, the governing equations (the differential form of Maxwell's equations) must be modified to include the tensor form of the conductivities and the conditions for reflectionless propagation. The typical electric and magnetic field equations become

$$\varepsilon \frac{\partial \mathcal{E}_{yx}}{\partial t} + (\sigma + \sigma_x)\mathcal{E}_{yx} + \Phi_{yx} = -\frac{1}{s_x}\frac{\partial \mathcal{H}_z}{\partial x} \tag{2}$$

$$\mu \frac{\partial \mathcal{H}_{yx}}{\partial t} + (\sigma^* + \sigma_x^*)\mathcal{H}_{yx} + \Psi_{yx} = -\frac{1}{s_x}\frac{\partial \mathcal{E}_z}{\partial x} \tag{3}$$

where

$$\frac{\partial \Phi_{yx}}{\partial t} = \frac{\sigma\sigma_x}{\varepsilon}\,\mathcal{E}_{yx}, \qquad \frac{\partial \Psi_{yx}}{\partial t} = \frac{\sigma^*\sigma_x^*}{\mu}\,\mathcal{H}_{yx} \tag{4}$$

[2] For example, when the soil is highly conducting, cutoff will occur whenever $h_a < \lambda_o/2$, where λ_o is the wavelength in free-space.

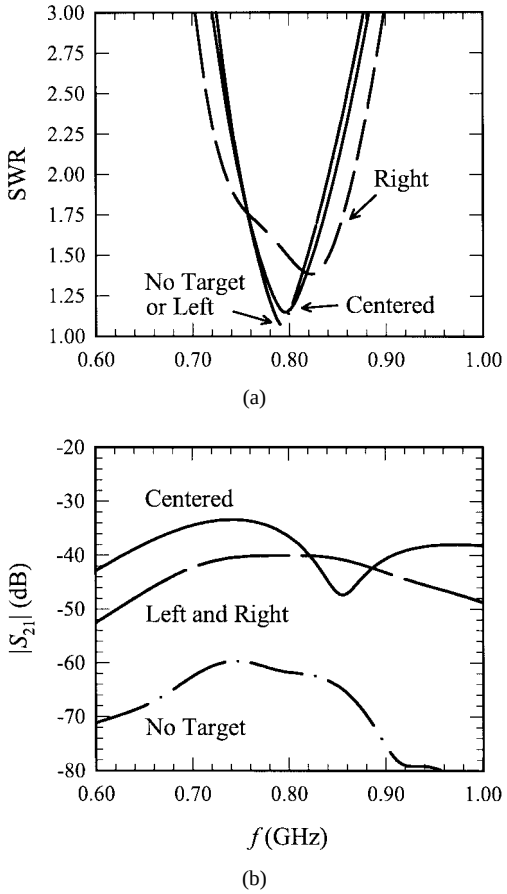

Fig. 3. FDTD results as sensor is shifted from left to right at height $h_a = 2.8$ cm over soil ($\varepsilon_r = 8.1$, $\sigma = 0.04$ S/m) containing a plexiglass block buried at depth $d_t = 7.6$ cm. (a) SWR. (b) $|S_{21}|$.

and $\sigma_x^* = \sigma_x \mu/\varepsilon$. The variables Φ_{yx} and Ψ_{yx} are introduced to simply help with the implementation of the GPML technique. Central differencing is used to write these equations in the standard form of the FDTD update equations. Reference [9] describes the above equations in greater detail. Because the problem is modeled on a parallel-processing computer, it is computationally simpler and more time efficient to use the same governing equations for all components in the grid. For this reason, the field components are split into subcomponents not just within the GPML but throughout the entire FDTD grid.

B. Computational Requirements

The FDTD simulation was performed on the CM-5 computer located at the Army High Performance Computing Center (AHPCRC) at the University of Minnesota. The CM-5 is optimized for data parallelism, a particular type of architecture in which many processors perform the same general formulas on many elements at the same time. This type of parallelism is particularly useful for the FDTD analysis. The parallel code is implemented on the CM-5 using connection machine FORTRAN (CM-FORTRAN), a special data-parallel language that provides a method for defining parallel data structures. The CM-5 consists of 832 Sparc processors each having 32 Mb of memory for a total of over 26 Gb of memory. The machine may be configured in partitions ranging from 64–512 processors, where the number of processors must be a power of two. When 512 processors are used, a program can store up to 16 Gb.

The FDTD volume that models the mine-detection problem contains 16.8 million cells and a total of about 906 million unknowns (54 per cell): 201 million electric and magnetic field components (12 per cell), 302 million electric field update coefficients (18 per cell), 201 million magnetic field update coefficients (12 per cell), 101 million GPML variables (6 per cell), and 101 million GPML update coefficients (6 per cell). Running the simulation requires about 3.9 Gb of memory. This is mainly the 3.6 Gb used to store the unknowns and the 230 Mb used to store the microcode. The program is generally run for 7500 time steps, which requires about 45 min of CPU time on a 256 processor partition of the CM-5. This number of time steps is sufficient to allow the ringing of the antennas to die out in order to obtain complete time signatures and accurate frequency domain results.

C. Results

The FDTD simulation was used to study the detection capabilities of the separated-aperture sensor under conditions (sensor height, target properties and depth, and soil properties) that might be encountered in searching for a buried nonmetallic mine. Here we will only present representative results from these simulations; the complete results are in [12].

For the cases discussed below, the soil is a Georgia red clay with 9.6% water by dry weight and the following measured constitutive parameters at 790 MHz: $\varepsilon_r = 8.1$, $\mu_r = 1.0$, $\sigma = 0.038$ S/m [13]. This particular soil is appropriate for a general study of the sensor operation, since the water content and electrical properties are in the medium range, i.e., the soil is neither completely dry nor saturated, resulting in mid-range values for ε_r and σ. The target is a plexiglass block ($30.5 \times 30.5 \times 7.3$ cm, with $\varepsilon_r = 2.6$, $\mu_r = 1.0$, $\sigma \approx 0$). This block has electrical properties similar to those of nonmetallic land mines, which generally have plastic exteriors (ε_r near 3) and TNT ($\varepsilon_r \approx 2.89$) as the primary filler [14]. The sensor height and target depth are 2.8 cm and 7.6 cm, respectively. The former gives good sensitivity, while the latter is a reasonable depth for a buried mine.

Results are obtained with the sensor over empty ground and as the sensor is moved from left to right over the buried target. In all cases, the antenna on the left side of the sensor (port 1) is transmitting, while the antenna on the right side of the sensor (port 2) is receiving. Fig. 3 shows the SWR and $|S_{21}|$ with the sensor over empty ground (dot-dash line) and with the sensor in each of three positions over the target: centered over the left edge of the target (long-dash line), centered over the target (solid line), and centered over the right edge of the target (short-dash line).

Notice that the antenna is well matched with the sensor over empty ground; the SWR is less than 1.1 at 790 MHz [Fig. 3(a)]. This match was obtained by adjusting the position of the metallic shorting plate on the stub. There is little effect on the SWR as the sensor is moved from left to right over the target until the sensor is positioned to the right of the target.

In this position, the target is directly below the transmitting antenna, and the field under this antenna is the most perturbed by the target, as is the SWR. However, even in this case, the SWR is less than 1.7 at 790 MHz.

$|S_{21}|$ increases as the sensor is shifted from a position over empty soil to a position over the left edge of the target to a position over the center of the target. $|S_{21}|$ then decreases as the sensor is shifted away from the target center toward a position over the right edge of the target. Notice that the target is clearly detectable for all three positions [Fig. 3(b)]; $|S_{21}|$ at 790 MHz is at least 20 dB greater than for the no target case for all three sensor positions over the target. Due to the reciprocity of the system, the curves for $|S_{21}|$ with the sensor shifted left (long-dash line) and right (short-dash line) of the target center are the same in Fig. 3(b).

Fig. 4 shows gray scale plots for the magnitude of the y-directed electric field, $|\mathcal{E}_y|$, on the x–z plane of symmetry for the frequency 790 MHz. The plots are for the sensor over empty soil, Fig. 4(a), for the sensor centered on the target, Fig. 4(b), and for the sensor centered over the right edge of the target, Fig. 4(c). These results were obtained by running the FDTD simulation with a ramped sinusoidal source of the form

$$\mathcal{V}(t) = V_o \exp\left[-\frac{1}{2}\left(\frac{3T-t}{T}\right)^2\right]\sin(\omega t), \qquad \text{for } t < 3T$$
$$= V_o \sin(\omega t), \qquad \text{otherwise} \tag{5}$$

where $V_o = 1$ V and $T = 1.26$ ns. The ramped sinusoid was introduced into the transmission line of the transmitting antenna and then the simulation was run long enough to allow the radiated and reflected fields to reach steady state. The values of $|\mathcal{E}_y|$ on the x–z plane were saved for a series of time steps. The stored data were then viewed as a movie using *The Data Visualizer*, a software visualization tool.[3] The gray-scale plots in Fig. 4 are "snapshots" (single frames) from the movies.

The same gray-scale levels are used for all three plots in Fig. 4. Scaled outlines of the sensor (dipoles, reflectors, and septum), the soil interface, the target, and the absorbing boundaries are imposed on the gray-scale plots. The left dipole (marked T) is the transmitting antenna and the right dipole (marked R) is the receiving antenna. Notice, in these plots there is no visible reflection from the GPML boundaries.

With the sensor over empty ground, Fig. 4(a), the field radiated by the transmitting antenna spreads out symmetrically into the ground. There is no visible coupling beneath the septum, nor is there a visible signal at the receiving antenna. The half-wavelength periodicity of $|\mathcal{E}_y|$ is evident. The presence of the target clearly perturbs the field when the sensor is centered on the target [Fig. 4(b)] and when the sensor is over the right edge of the target [Fig. 4(c)]. In both cases, the field can be seen between the septum and the surface of the ground as well as between the surface of the ground and the top of the block. In some sense, this field may be guided by the parallel, planar elements of the structure (septum, surface of the ground, and the top of the block). There is a visible field at the receiving antenna with the target present, and this signal is larger (darker) with the sensor centered on the target than with the sensor shifted to the right. These gray-scale plots indicate a minimum received signal when the sensor is over empty ground, a maximum when the sensor is centered over the target, and a signal intermediate to these two levels when the sensor is over the edge of the target; this is consistent with the results in Fig. 3(b) for $|S_{21}|$ at 790 MHz.

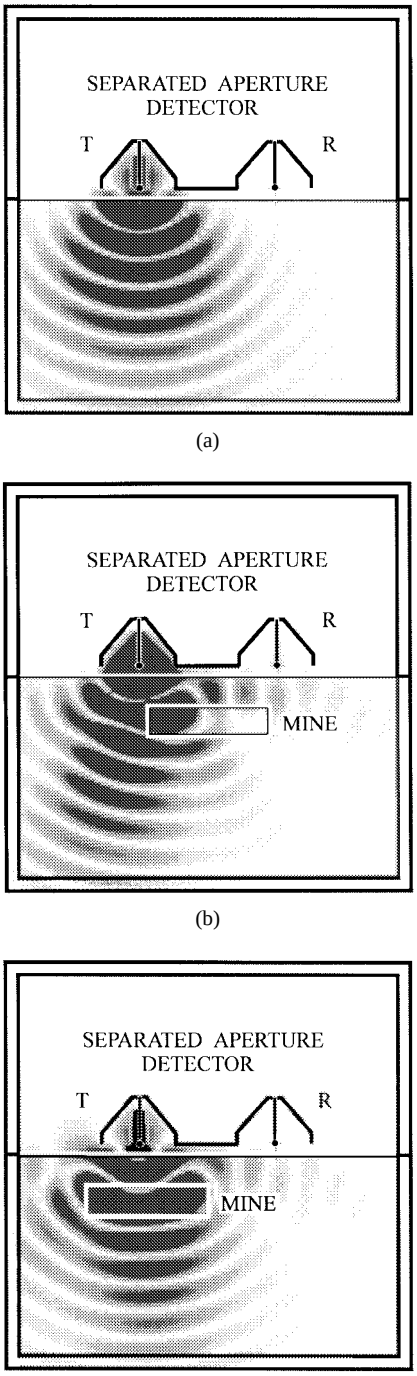

Fig. 4. Gray-scale plots of $|\mathcal{E}_y|$ at 790 MHz on plane of symmetry. (a) Sensor over empty soil. (b) Sensor centered on target. (c) Sensor centered over right edge of target.

[3] *The Data Visualizer* is a registered trademark of WaveFront Technologies, Inc.

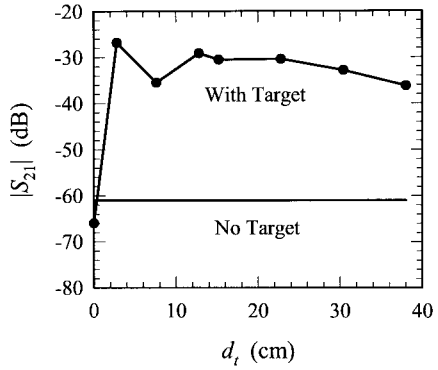

Fig. 5. FDTD results for $|S_{21}|$ at 790 MHz as a function of target depth d_t with sensor centered over target at height $h_a = 2.8$ cm.

The FDTD simulation provides an efficient means for performing studies of the effects of variation in problem parameters such as the sensor height, soil properties, and target properties. To perform a parametric study, a set of problem parameters defining a control case is chosen. Then results are obtained as one of the parameters (such as the target depth) is varied while the others are held constant. The FDTD simulation of the separated-aperture sensor has been used to perform parametric studies of the effects of variation in sensor height, target depth, and soil properties. Complete results from these studies are presented in [12]. Some results will be shown here from the parametric study of variation in target depth.

The problem parameters from the preceding discussion were used as the control case, since these are reasonable parameters for the mine detection problem. The FDTD simulation was run with all of these parameters held constant while the depth of the plexiglass block was varied from $d_t = 0$ to 38 cm. The antennas were matched at 790 MHz over empty ground, and the SWR was less than 1.25 with the target at any depth.

Fig. 5 shows the calculated $|S_{21}|$ at 790 MHz versus target depth. These results show a rapid increase in $|S_{21}|$ as the target depth is increased from 0 to 2.8 cm, then, after minor oscillation, a monotonic decrease in $|S_{21}|$ with increasing target depth. The small magnitude of $|S_{21}|$ for the flush target, $d_t = 0$, is probably due to destructive interference between signals scattered from the block and directly coupled between the antennas. For all target depths greater than 2.8 cm, the increase in $|S_{21}|$ due to the presence of the target is greater than 23 dB. These results show the ability of the sensor to detect a dielectric target over a wide range of depths.

IV. Comparison to Measurements

The FDTD simulation of the mine-detection system is quite complex, so it is very important to verify both the accuracy of the models used for the components and the implementation of these models on the computer. The component parts of the problem were tested individually [12]. For example, the method for feeding the antennas was checked, both on transmission and reception, by comparison with published data (input impedance and effective height) for dipole antennas in free-space, and the operation of the absorbing boundary was checked by examining the field of an electrically short dipole placed over an air-ground interface in a box with walls covered by the GPML. The ultimate test for the simulation, however, is a comparison of computed results with measurements made using an actual detector; this is the subject of this section.

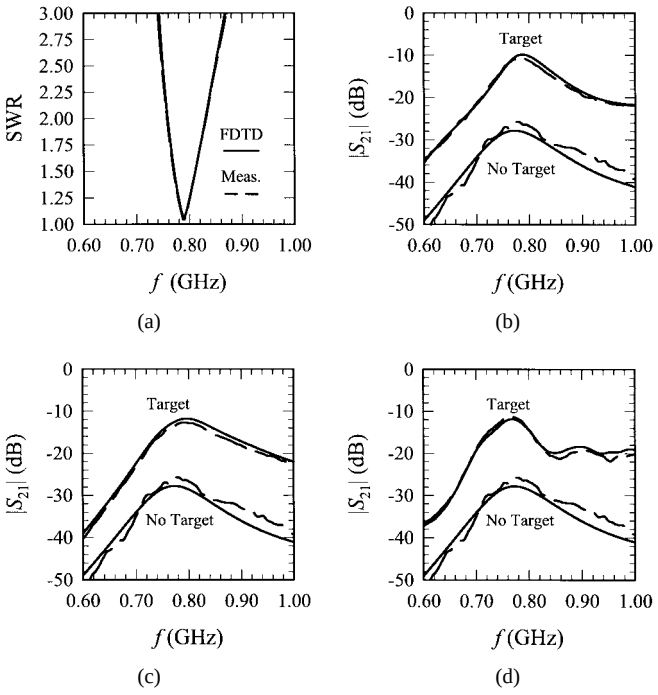

Fig. 6. Theoretical (FDTD) results compared to measurements for sensor in air over low-frequency electromagnetic absorber. (a) SWR no target. (b) $|S_{21}|$ for aluminum plate. (c) $|S_{21}|$ for plexiglass block. (d) $|S_{21}|$ for Stycast block.

A. Sensor Above Absorber—Georgia Tech Measurements

A separated-aperture sensor with the dimensions shown in Fig. 1 was constructed at Georgia Tech. Measurements were made with this sensor in air 29.2 cm above low-frequency absorber. The sensor was connected to a Hewlett-Packard network analyzer (Model 8510) used to measure the S parameters over the range of frequencies 0.5–1.5 GHz. With no target present, the tuning screw on the stub of each antenna was adjusted to obtain the lowest possible SWR at 790 MHz. The S parameters were then obtained with no target present and with a target centered below the sensor. A variety of objects were used as targets [12]. Here, results will be presented for three different targets: an aluminum plate (30.5 × 30.5 × 0.3 cm), a plexiglass block (30.5 × 30.5 × 7.3 cm, $\varepsilon_r = 2.6$), and a Stycast[4] block (30.5 × 30.5 × 6.8 cm, $\varepsilon_r = 7.4$). Notice that these cases represent extremes: a large metallic target, an all-dielectric target of low permittivity, and an all-dielectric target of high permittivity. For each target, the depth (distance from the sensor) was adjusted to maximize the coupling ($|S_{21}|$) at 790 MHz.

Fig. 6 presents comparisons of the FDTD results (solid lines) with the measurements (dashed lines) for four cases: SWR and $|S_{21}|$ for no target [Fig. 6(a), (b)], and $|S_{21}|$ for a metal plate 28.9 cm below the sensor [Fig. 6(b)], a plexiglass block 7.2 cm below the sensor [Fig. 6(c)], and a Stycast

[4] Stycast is a registered trademark of Emerson & Cumings, Inc.

block 8.4 cm below the sensor [Fig. 6(d)]. Each of the graphs is for a range of frequency (0.6–1.0 GHz) centered about the resonant frequency, 790 MHz. In all cases, the FDTD results are in good agreement with the measurements. The changes in $|S_{21}|$ associated with the different targets are clearly predicted by the simulation. The values of $|S_{21}|$ at 790 MHz for the various arrangements are: no target, -28 dB for the simulation versus -26 dB for the measurement; metallic plate, -10 dB versus -11 dB; plexiglass block, -12 dB versus -13 dB; Stycast block -13 dB versus -13 dB. The overall good agreement shows that the simulation properly models the sensor (antennas, antenna feeds, stubs, and corner reflectors), and target and that the absorbing boundary condition (GPML) is effectively truncating the lossless medium (free-space).

The results in Fig. 6 are for the range of frequencies 0.6–1.0 GHz. Results were also computed and measured over the wider range 0.5–1.5 GHz, and the agreement is equally good [12]. These broad-band results show target-dependent structure in $|S_{21}|$ not seen in Fig. 6. This structure might be useful for target identification.

B. Sensor Above Soil—United States Army Measurements

FDTD simulations were performed for comparison with some of the Army's experimental results. Fig. 7 shows FDTD results for the experiment described in Section II. The agreement between the FDTD results in Fig. 7 and the Army's measured results in Fig. 2 is fairly good. Both predict a significant increase in $|S_{21}|$ as the sensor is moved over the buried target. The major differences are that the antennas in the simulation are better matched (lower SWR at 790 MHz), and that $|S_{21}|$ with the target absent is lower in the simulation. Both of these differences are understandable. It is much easier to tune the antennas in the simulation; one does not have to pick up the antennas, turn them over, tune them, then replace them over the ground as in the experiment; hence, it is easier to obtain a lower SWR in the simulation. In the experiments, the elements of the sensor may have been slightly asymmetric, the surface of the soil may have been rough, and inhomogeneities may have been present in the soil. All of these factors could increase the coupling $|S_{21}|$ in the experiment with the target absent. Notice that in both cases $|S_{21}|$ with the target absent is very small: in the experiment $|S_{21}| < -50$ dB, and in the simulation $|S_{21}| < -60$ dB.

Another factor that could influence this comparison is the accuracy of the measured values for the electrical parameters of the soil. The values of relative permittivity for the target (nylon block) and soil are very close ($\varepsilon_r = 3.16$ versus $\varepsilon_r = 2.9$); hence, only a small error in the measured permittivity for the soil could greatly change the dielectric contrast between the soil and the target. For example, if the permittivity of the soil were only 9% higher, it would be the same as the permittivity of the target and the target would be undetectable (assuming the slight difference in the conductivities of the target and soil cannot be used for detection). Also, the measured relative permittivity, $\varepsilon_r = 2.9$, for the soil appears to be low for the quoted water content, 6% by weight. Measurements on a comparable soil (bulk density 1.5 gm/cm^3) with a water content of 5% by dry weight give $\varepsilon_r \approx 5.0$ and $\sigma \approx 2 \cdot 10^{-2}$ S/m [13].

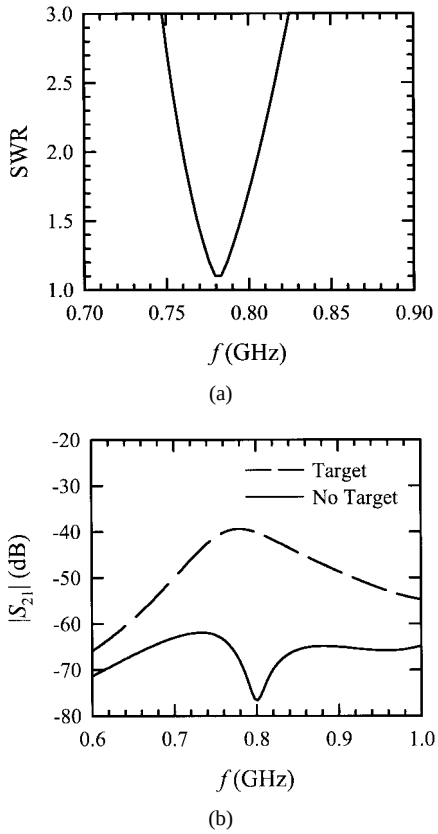

Fig. 7. FDTD results with separated-aperture sensor at height $h_a = 7.6$ cm over soil. (a) SWR. (b) $|S_{21}|$ for sensor over empty soil (no target) and over soil containing a nylon block buried at depth $d_t = 7.6$ cm. Results are to be compared to United States Army measurements in Fig. 2.

V. Conclusions

This paper shows that the FDTD method can be used to accurately simulate the complete electromagnetic performance of a mine-detection sensor. The results demonstrate that the FDTD simulation is a powerful tool capable of replacing experimentation in the initial design and optimization of such sensors. The particular simulation described in this paper is a one-of-a-kind process requiring a supercomputer; however, as the speed and memory of computers increase and the details of the FDTD method become standard, such simulations will become routine.

The simulations discussed in this paper included a generic model for the nonmetallic mine (dielectric block) and a homogeneous ground. The flexibility of the FDTD method, however, makes it easy to include specific details of the mine, such as the fusing mechanism, air pockets, etc., and any structure in the ground, such as stratification, rocks, surface roughness, etc.

In this paper, the FDTD method was used to model a narrow-band sensor. However, because of its time-domain basis, the method is ideally suited to model broad-band or ultrawide-band sensors [15].

ACKNOWLEDGMENT

The authors would like to thank Dr. J. Fang for the preprint of his paper on the GPML, Dr. W. Scott, Jr., and Dr. W. Humbert for measuring the relative permittivity of the Stycast material, and the Georgia Tech Graphics, Visualization, and Usability Center for providing tools to make movies and gray-scale plots. They would also like to thank C. A. Amazeen and Dr. L. S. Riggs for discussing the United States Army's measurements with the separated-aperture sensor.

REFERENCES

[1] B. Boutros-Ghali, "The land mine crisis," *Foreign Affairs*, vol. 73, no. 5, pp. 8–13, Sept./Oct. 1994.
[2] "Basic studies-detecting, destroying or inactivating mines," US Army Eng. Ctr, Fort Belvoir, VA, Final Rep., Contract DA-44-009 Eng-1773, Nov. 1953.
[3] C. Stewart, "Summary of mine detection research, vol. 1 and 2," US Army Eng. Res. Development Labs., Fort Belvoir, VA, Tech. Rep. 1636, May 1960.
[4] R. V. Nolan, H. C. Egghart, L. Mittleman, R. L. Brooke, F. L. Roder, and D. L. Gravitte, "MERADCOM mine detection program 1960–1980," US Army Mobility Equipment Res. Development Command, Fort Belvoir, VA, Rep. 2294, Mar. 1980.
[5] G. S. Smith, "Summary Report: Workshop on new directions for electromagnetic detection of nonmetallic mines," US Army Belvoir Res., Development, Eng. Ctr., Countermines Syst. Directorate, Fort Belvoir, VA, TCN 92153, June 1992.
[6] L. S. Riggs and C. A. Amazeen, "Research with waveguide beyond cutoff or separated-aperture dielectric anomaly detection scheme," US Army Belvoir Res., Development, Eng. Ctr., Tech. Rep. 2497, Aug. 1990.
[7] K. S. Yee, "Numerical solution of initial boundary value problems using Maxwell's equations in isotropic media," *IEEE Trans. Antennas Propagat.*, vol. AP-14, pp. 302–307, May 1966.
[8] A. Taflove, *Computational Electrodynamics: The Finite-Difference Time-Domain Method.* Boston, MA: Artech House, 1995.
[9] J. Fang and Z. Wu, "Generalized perfectly matched layer—An extension of Berenger's perfectly matched layer boundary condition," *IEEE Microwave Guided Wave Lett.*, vol. 5, pp. 451–453, Dec. 1995.
[10] K. R. Umashankar, A. Taflove, and B. Beker, "Calculation and experimental validation of induced currents on coupled wires in an arbitrary shaped cavity," *IEEE Trans. Antennas Propagat.*, vol. AP-35, pp. 1248–1257, Nov. 1987.
[11] J. M. Bourgeois and G. S. Smith, "A fully three-dimensional simulation of a ground-penetrating radar: FDTD theory compared with experiment," *IEEE Trans. Geosci. Remote Sensing*, vol. 34, pp. 36–44, Jan. 1996.
[12] J. M. Bourgeois, "A complete three-dimensional electromagnetic simulation of ground-penetrating radars using the finite-difference time-domain method," Ph.D. dissertation, Georgia Inst. Technol., Atlanta, GA, Jan. 1997.
[13] W. R. Scott, Jr. and G. S. Smith, "Measured electrical constitutive parameters of soil as functions of frequency and moisture content," *IEEE Trans. Geosci. Remote Sensing*, vol. 30, pp. 621–623, May 1992.
[14] "Instruction sheet: Target, mine detection, EM inert," VSE Corp., Alexandria, VA 22303, Rep.
[15] T. P. Montoya, "Vee dipole antennas for use in short-pulse ground-penetrating radars," Ph.D. dissertation, Georgia Inst. Technol., Atlanta, GA, Mar. 1998.

Jacqueline M. Bourgeois (S'87–M'98) was born in Gulfport, MS, on May 23, 1965. She received the B.E.E. degree (highest honors) from the Georgia Institute of Technology, Atlanta, GA, in 1988, and the M.E.E. and Ph.D. degrees in electrical engineering from Georgia Tech, Atlanta, in 1996 and 1997, respectively.

From 1997 to 1998, she was employed as an Electronics Engineer Specialist with the Antenna Products Center of Lockheed Martin Missiles and Space, Sunnyvale, CA. She is currently employed as a Senior Design and Development Engineer with the Missile Radar Laboratory, Raytheon Systems Company, Sudbury, MA. Her technical interests include numerical methods in electromagnetics, theory, design, and development of antenna and microwave elements, and design and development of phased-array antennas.

Glenn S. Smith (S'65–M'72–SM'80–F'86) received the B.S.E.E. degree from Tufts University, Medford, MA, in 1967, and the S.M. and Ph.D. degrees in applied physics from Harvard University, Cambridge, MA, in 1968 and 1972, respectively.

From 1972 to 1975, he served as a Postdoctoral Research Fellow at Harvard University and also as a part-time Research Associate and Instructor at Northeastern University, Boston, MA. In 1975 he joined the faculty of the Georgia Institute of Technology, Atlanta, GA, where he is currently Regents' Professor of Electrical and Computer Engineering. He is author of *An Introduction to Classical Electromagnetic Radiation* (Cambridge, U.K.: Cambridge Univ. Press, 1997) and coauthor of the book *Antennas in Matter: Fundamental, Theory and Applications* (Cambridge, MA: MIT Press, 1981). He also authored the chapter "Loop Antennas" in *Antenna Engineering Handbook* (New York: McGraw-Hill 1993). His technical interests include basic electromagnetic theory and measurements, antennas, and wave propagation in materials, and the radiation and reception of pulses by antennas.

He is a member of Tau Beta Pi, Eta Kappa Nu, and Sigma Xi. He is also a member of URSI Commissions A and B.